Earthquake magnitude estimation from peak amplitudes of very early seismic signals on strong motion records

Aldo Zollo,[1] Maria Lancieri,[1] and Stefan Nielsen[2]

[1]   We show that the low-pass filtered, peak amplitudes of initial P- and S-wave seismic signals recorded in the vicinity of an occurring earthquake source correlates with the earthquake magnitude and may be used for real-time estimation of the event size in seismic early warning applications. The earthquake size can be therefore estimated using only a couple of seconds of signal from the P- or S-wave onsets, i.e. while the rupture itself is still propagating and rupture dimension is far from complete. We argue that dynamic stress release and/or slip duration on the fault in the very early stage of seismic fracture, scales both with the observed peak amplitude and with the elastic energy available for fracture propagation. The probability that a fracture grows to a larger size should scale with the energy initially available. **Citation:** Zollo, A., M. Lancieri, and S. Nielsen (2006), Earthquake magnitude estimation from peak amplitudes of very early seismic signals on strong motion records, *Geophys. Res. Lett.*, *33*, L23312, doi:10.1029/2006GL027795.

1.   Introduction

[2]   Over the last few decades, there has been ongoing experimentation into earthquake early warning (EEW) systems in several active seismic areas of the world. Prototype EEW systems have been developed and implemented in Taiwan, Japan, USA and Mexico, with the basic idea that alert signals from dense seismograph networks in the earthquake source areas could be sent to nearby urban settlements several tens of seconds in advance of the arrival of destructive seismic waves.

[3]   The main infrastructure of regional EEW systems [*Kanamori*, 2006] is constituted by a dense seismic network deployed in the potential earthquake source area. The earthquake-warning window begins at the time of the first P-wave detection by the network and it can last from a few to several tens of seconds, depending on the distance between the source and the alert target area. In this case, fully automated, robust and reliable real-time estimates of the main earthquake parameters (location and magnitude) must be obtained in an evolving, continually updated form, so that they can be used for warning purposes or to rapidly simulate reliable shake maps, and be helpful for managing emergency actions.

[4]   In order to provide real-time magnitude estimations for EEW purposes, a method based on the predominant period (τ_p) measured over a narrow time window (4 seconds) extending from just after the first P-wave arrival has been first proposed by *Allen and Kanamori* [2003]. The method has been mainly validated and calibrated on regional recordings of velocity ground motion.

[5]   The evidence for a scaling relationship between the parameter τ_p and magnitude observed on earthquake records from different seismic regions led recently *Olson and Allen* [2005] to argue about the deterministic nature of the rupture process, allowing to predict the earthquake size from the measurement of frequency content of early radiated seismic signals. This hypothesis is called in question by *Rydelek and Horiuchi* [2006] who found no evidence of dominant frequency scaling with magnitude from the analysis of waveform data recorded by the Japanese Hi-net seismic network.

[6]   Using an alternative approach, *Wu and Zhao* [2006] determined an attenuation relationship for low-pass, filtered peak displacement amplitude (P_d) measured in the first three seconds after the arrival of the P-wave, based on southern California earthquake waveform data. They show that P_d is a robust measurement for estimating the magnitudes of earthquakes and has practical application in earthquake early warning systems.

[7]   During the last two decades, the availability of wide-dynamic, high density accelerometric networks deployed in active seismic areas provided for detailed information on the earthquake rupture process and on the areal distribution on strong ground shaking soon after moderate to large events. In Italy a dense accelerometric network is being deployed on the earthquake causative fault systems in the southern Apenninic belt region which represents the basic infrastructure of an earthquake early warning system under development for the Campania-Lucania region [*Weber et al.*, 2006].

[8]   In this study we show the advantages of using near-source strong motion records for real time estimation of earthquake magnitude. In fact they provide unsaturated recordings of moderate to large earthquakes and, in case of dense station coverage of the source area, the combination of both P- and S-wave amplitude information can be used to get fast and robust earthquake location and magnitude estimates. We demonstrate the statistically significant scaling between the early peak amplitude of the seismic signal, and the earthquake final magnitude. We discuss the implications of this result for the physics of rupture, in terms of stress drop $\Delta\sigma$, fracture dimensions L and energy flow G.

2.   Data Analysis

[9]   In the present study we analyze 376 three-component records from the European Strong-Motion Database (ESD)

[1]Dipartimento di Scienze Fisiche, Università di Napoli Federico II, Naples, Italy.
[2]Istituto Nazionale di Geofisica e Vulcanologia, Rome, Italy.
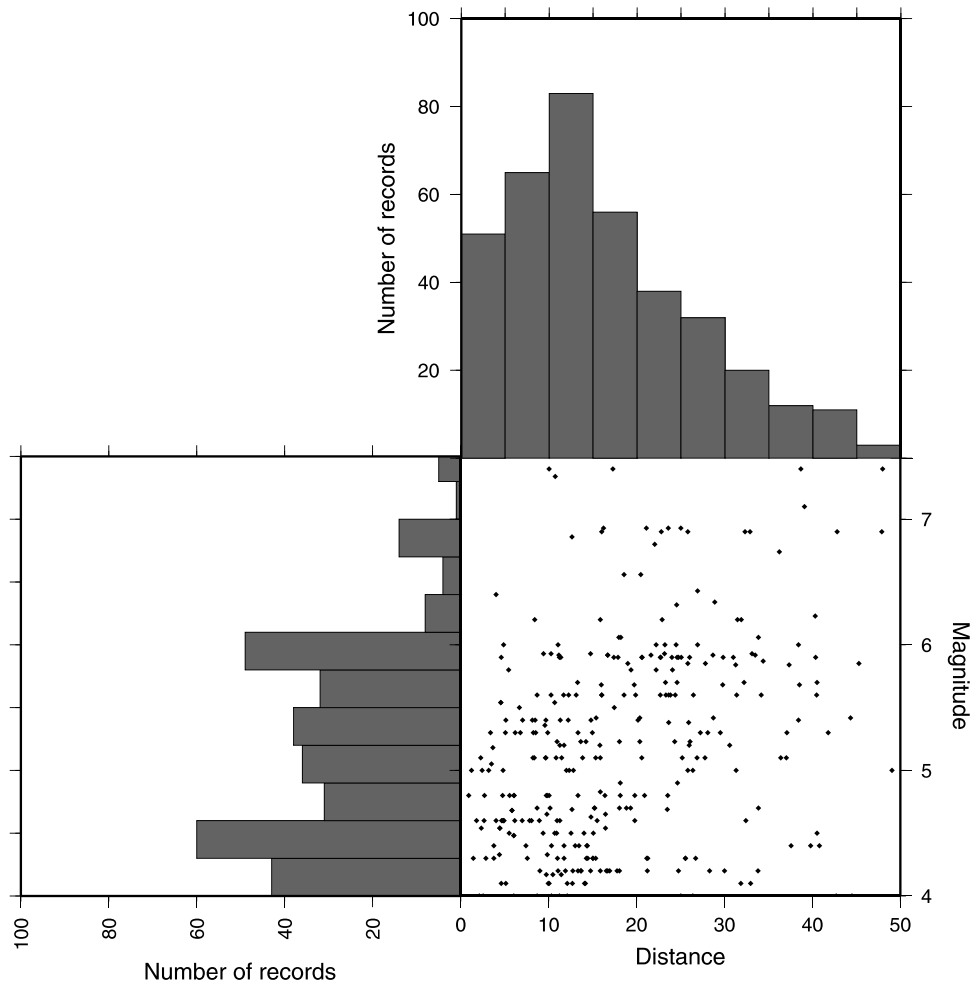
Figure 1. Data distribution vs magnitude and epicentral distance. (top) Histogram of the number of selected strong motion records with magnitude. An interval of 0.3 is used for each magnitude bin. (bottom left) Distribution of records (diamonds) vs distance and magnitude. (bottom right) Histogram of the number of selected strong motion records with distance. An interval of 5 km is used for each distance bin.

[*Ambraseys et al.*, 2004], relative to 207 moderate-to-large earthquakes ($4 \leq M_W \leq 7.4$) that have occurred overall the Mediterranean basin in the period 1976–1999 (Figure S1 in auxiliary material[1]).

[10] Only records at epicentral distances smaller than 50 km have been considered for the analysis, based on the general observation that high-frequency, direct body waves radiating from crustal earthquake ruptures dominate in amplitude within the near-source range, i.e. at receiver distances comparable with the earthquake rupture length [*Zeng et al.*, 1993].

[11] For all the considered events we re-assigned the earthquake magnitude using the CMT Harvard moment magnitude catalogue.

[12] For earthquakes with $M_W \geq 6.5$ the EDS hypocentral coordinates have been re-compiled by using the updated estimates available from specific studies and from National

Geophysical Data Center (NGDC) catalogue (Table S1 in auxiliary material).

[13] The analyzed events occurred along the whole active seismic belt of the Mediterranean region, encompassing different geological and tectonic contexts and being associated to various types of faulting mechanisms.

[14] Distributions of the number of analyzed strong-motion records as a function of moment-magnitude and epicentral distance are displayed in Figure 1. Most records are at distances less than 20 km from the source. In the following analysis, the data are grouped in magnitude classes of width equal to 0.3, this value roughly corresponding to the mean error for standard magnitude estimates. Each magnitude class contains records originating from various earthquakes occurring in different tectonic regimes, thus averaging out effects on peak amplitudes due to the fault mechanism and rupture directivity.

[15] The ESD data processing involves digitization, sensitivity correction, linear base-line correction and filtering in the frequency band 0.25 to 25 Hz. After a series of trials using different low-pass corner frequencies, we chose to apply a zero-phase-shift, low-pass Butterworth filter with a

---

[1]Auxiliary material data sets are available at ftp://ftp.agu.org/apend/gl/ 2006gl027795. Other auxiliary material files are in the HTML.
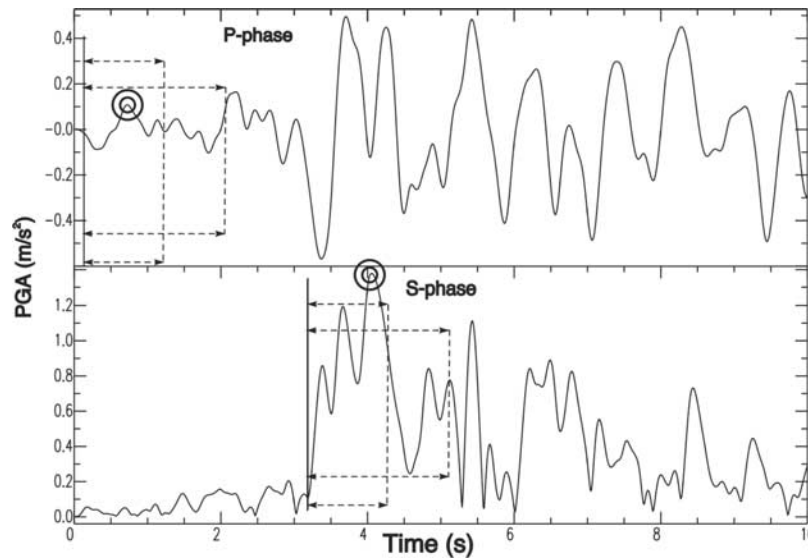
Figure 2. Analysis of strong-motion records for the measurement of peak ground motion values. The figure displays the 3Hz low-pass filtered displacement records of the 1980, Irpinia earthquake (M = 6.9) by station BGI (Bagnoli Irpino) located at an epicentral distance of 22 km. (top) Plot of the vertical component used to measure P-peak data. The maximum amplitude (open circles) is measured in time windows of 1 and 2 seconds after the estimated first P-arrival. (bottom) Plot of the modulus of the horizontal component, defined as $H(t) = \sqrt{NS^2(t) + EW^2(t)}$ where $NS(t)$ and $EW(t)$ are the North-South and East-West components, respectively. This plot is used to measure S-peak data (open circles) in time windows lasting 1 and 2 seconds after the first S-arrival, manually picked on horizontal records.

corner frequency of 3Hz, which provided the best results in terms of the correlations between the observed ground-motion quantities and moment magnitudes. This particular choice is justified by the fact that for waveform analysis noncausal filters preserve the shape and amplitude of waveforms better than, for instance, causal filters which are generally used to preserve onset timing information [*Gubbins*, 2004].

[16] The first S-arrivals from the horizontal components of all of the selected strong-motion records has been identified and manually picked. The S-signal detection is based on the analysis of variation of amplitude, frequency and horizontal polarization as functions of time along the low-pass filtered accelerograms.

[17] The expected first P-arrival time (T_P) and triggering (or first sample) time (T_{FS}) are therefore calculated from the first S-wave reading using a homogeneous crustal velocity model, with $v_p = 5.5$ km/s and $v_s = 3.2$ km/s. This procedure is particularly relevant for analogue records for which a pre-triggering window is not available. The records have been classified according to the estimated $T_S - T_P$ times and $T_{FS} - T_P$. The large majority of analyzed records shows S-P times smaller than 3 sec and a first P-arrival within ±1 sec from the triggering time of strong motion records.

[18] Starting from the estimates of first P-wave and manually picked S-wave arrivals, we considered two different time windows, 1 and 2 sec wide, on the low-pass filtered records where to measure the peak ground displacement value (PGD_t, where the subscript t is for 1- or 2-sec) (Figure 2).

[19] Due to the uncertainty in the identification of the first P arrival time, only the 2-sec window has been considered for P-wave peak measurements, while both 1-sec and 2-sec windows are used for S-waves.

3. Correction for Distance Attenuation

[20] In order to correct the early P- and S-wave peak amplitude for the distance attenuation effect, we assumed a simple linear relationship between the logarithmic PGD_t, the magnitude and the logarithmic hypocentral distance [*Wu and Zhao*, 2006]:

$$\log(PGD_t) = f(M, R) = C + B \cdot M + A \log(R) \qquad (1)$$

where the constants A, B and C have been determined through a best-fit regression analysis. The coefficients of the estimated curves are reported in Table 1.

[21] The last column of Table 1 reports the retrieved standard errors (SE). The SE and error estimates on coefficients in Table 1 account for unknown source and/or path effects which are not considered in equation (1), as radiation pattern, source directivity and site effects.

[22] In order to retrieve the magnitude dependence of early P- and S-peak amplitudes, we used equation (1) to correct the observed peak amplitudes for the distance effect, by normalizing them to a reference distance of 10 km. This

Table 1. Coefficients of Estimated Curves Along With Retrieved Standard Errors

	A	*B*	*C*	*SE*
P − 2 sec	−1.05 ± 0.3	0.81 ± 0.06	−5.97 ± 0.48	0.6
S − 1 sec	−0.71 ± 0.17	0.51 ± 0.04	−4.09 ± 0.23	0.4
S − 2 sec	−0.71 ± 0.16	0.56 ± 0.04	−4.253 ± 0.22	0.4
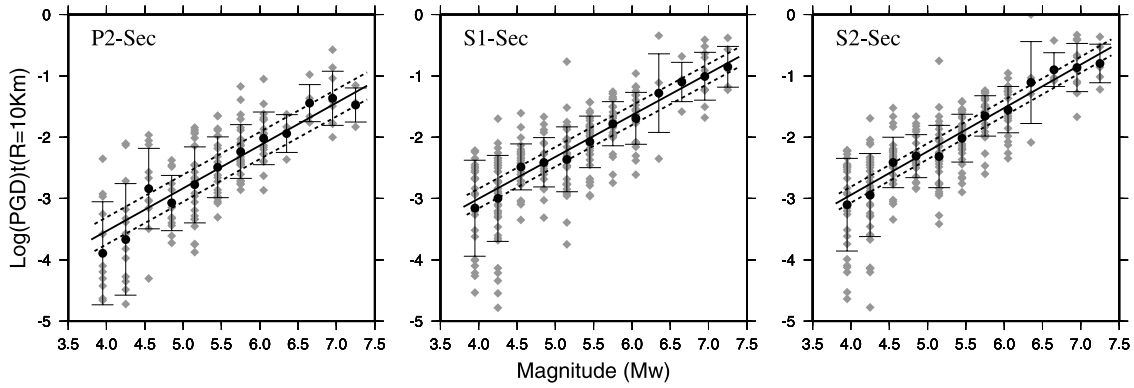
Figure 3. Correlation between low-pass filtered peak ground motion value and moment-magnitude. The panels show the logarithm of peak ground displacement normalized at a reference distance of 10 km as a function of M_w in time windows of (left) 2 sec length from the first P-arrival and (middle) 1- and (right) 2- sec from the first S-arrivals. P- and S-data are measured on vertical and root-squared sum of horizontal components, respectively. Each panel shows the best fit regression line (solid line) along with 1-WSE limits (dashed lines). The weighted standard error (WSE) is computed as

$$WSE = \sqrt{\frac{\sum_i w_i \left(\log\left(PGD_i^{10km}\right)\right) - A' - B'M_i}{\sum_i w_i}}$$ with $w_i = 1/\sigma_i$ (σ_i is the standard error on $\log(PGD_i^{10km})$ in each

magnitude bin), A' and B' are the retrieved best-fit line parameters.

values has been chosen as an approximate average of hypocentral distances for the analysed data set.

[23] For each bin in the earthquake magnitude range, the mean and standard deviation of distance corrected logarithmic peak displacement ($\log(PGD_t^{10km})$) have been computed. The single data points and the average values of $\log(PGD_t^{10km})$ as a function of magnitude for P- and S-wave signals are shown in Figure 3.

[24] A linear regression curve of the form:

$$\log\left(PGD_t^{10km}\right) = A' + B'M \qquad (2)$$

has been determined using the average values of $\log(PGD_t^{10km})$ in each magnitude bin weighted by the inverse of standard deviation. The single measurements and average estimates of $\log(PGD_t^{10km})$ along with error bars and best-fit regression (including the $\pm$ 1-WSE, weighted standard error, lines) are shown in Figure 3 while the values of parameters A' and B' are reported in Table 2 along with the measured weighted standard error.

[25] Even considering very short lapse times from the first P- and S-arrivals, the logarithm of peak ground motion quantities shows a striking linear correlation with magnitude both for P- and S-waves (correlation coefficients greater than 0.9) in the considered magnitude range ($4 \leq M_w \leq 7.4$). The statistical error on magnitude estimates using the retrieved regression model can be obtained by the weighted standard deviation between observed and predicted logarithms of ground motion quantities. Both for P- and S-waves this value generally decreases with the time window length and are rather stable with time even considering larger time windows both for P- and S-waves.

4. Discussion and Conclusions

[26] The presented results suggest that estimations of earthquake magnitude in real-time procedures can be

obtained by combining measurements from initial P- and S-wave signals as a function of time from the first P-wave detection.

[27] The use of S-wave data for early warning application is feasible in case of a dense strong-motion network is deployed around the potential earthquake source area (hypocentral distance smaller than $20–30$ km), so that first S-P times are smaller than $2–3$ seconds. Equation (2) can be usefully adopted to get real-time estimation of magnitude, if the hypocentral distance can be determined using real-time location procedures as, for instance, the method proposed by *Horiuchi et al.* [2005].

[28] *Wu and Zhao* [2006] pointed out the possible existence of a saturation effects of the early P-peak displacement amplitude vs Magnitude relationship for $M > 6.5$. Due to the limited data coverage for this magnitude range, we cannot argue about a similar effect on the analyzed European data-set.

[29] About the causative link between the initial displacement peak amplitude and the final magnitude of an earthquake, one hypothesis may be proposed as follows. Given that the peak ground displacement depends on the relatively high frequency content of the signal, that the receivers are not in the immediate vicinity of the rupturing fault, and that the effect of rupture directivity is averaged by the variable azimuthal position of the stations, the seismic radiation can be assimilated in first approximation to the far-field effect of a point source. In this case, P-wave radiation predicts a

Table 2. Values of Parameters A' and B' Along With Measured Weighted Standard Error

	A'	B'	WSE
$P − 2$ sec	$−6.31 \pm 0.37$	0.70 ± 0.06	0.22
$S − 1$ sec	$−5.72 \pm 0.17$	0.68 ± 0.03	0.16
$S − 2$ sec	$−5.77 \pm 0.24$	0.71 ± 0.04	0.13

ground motion $u(t)$ at a distance r from the source proportional to the moment rate [*Aki and Richards*, 1980]:

$$u(t) = \frac{A^{FP}}{4\pi\rho\alpha^3 r}\dot{M}_o\left(t - \frac{r}{\alpha}\right)$$

where the A^{FP} coefficient describes radiation angular dependence, and ρ is the mass density of the medium. The moment rate is:

$$\dot{M}_o = \mu\Delta\dot{u}\Sigma = \mu\Delta\dot{u}CL^2$$

for a given average slip-rate $\Delta\dot{u}$ over an active slip surface $\Sigma = CL^2$ (μ is the shear modulus, L is a linear crack dimension and C a geometrical factor of the order of 1).

[30] According to theoretical models of rupture dynamics [*Kostrov*, 1964; *Scholz*, 1990], the slip-rate amplitude scales linearly with dynamic stress drop $\Delta\sigma$. For example the slip rate at the centre of an expanding crack is $\Delta\dot{u} = h\left(\frac{v_r}{\beta}\right)\beta\frac{\Delta\sigma}{\mu}$ where β is the shear wave velocity and h is a dimensionless function of rupture velocity v_r. In addition, the earthquake fracture advancement is controlled by the flow rate of elastic energy G (in $J.m^{-2}$), which can be written as a function of stress drop and of the length L of actively slipping area (crack or fracture pulse), as:

$$G = f\left(\frac{v_r}{\beta}\right)\frac{\Delta\sigma^2}{\mu}L$$

where f is a dimensionless function depending on fracture velocity and loading conditions. The complex structure of the function $f\left(\frac{v_r}{\beta}\right)$ is not relevant here since it is independent of both L and $\Delta\sigma$. Further details are given by, for example, *Broberg* [1999] and *Nielsen* [2006].

[31] We see that both the far field displacement $u(t)$ and the energy flow G controlling rupture advancement, increase with stress drop and fracture length. Fractures with higher energy flow G have more chances of propagating across stronger patches of an earthquake fault. As a consequence, we may surmise that earthquake fractures with higher dynamic stress drop and/or active surface at their initiation, have an increased probability of propagating to larger distances and radiate larger wave amplitudes, as seen from the peak ground motion in the early portion of near-source P and S-signals. Of course, the statement is only true in a probabilistic sense, because the propagation of fracture also depends on the relative strength or weakness of the fault zones encountered (in terms of energy dissipated in friction and fracture growth). Even assuming an inhomogeneous strength distribution of faults, fractures releasing a larger amount of energy in the initial stage, are statistically prone to propagate over larger distances before they encounter a stopping barrier of sufficient strength. The energy balance argument should at least explain the trend observed in a catalog of several tens of earthquakes, though not reliable in a strictly the deterministic sense.

[32] One important implication of our experimental results is that stress drop and/or active slip surface have to scale with seismic moment in the initial stage of seismic ruptures.

[33] Specifically concerning stress release estimates performed on strong motion records, *De Natale et al.* [1987] show a significant dependence of Brune' stress drop [*Brune*, 1970] with moment, based on data sets from different worldwide earthquake sequences with $10^{11} \leq M_o \leq 10^{18}$ Nm, which they interpreted as an effect of violation in self-similarity of the moment vs fault size scaling law. More recently, *Beeler et al.* [2003] observe that apparent stress and Brune' stress drop co-vary with magnitude in the moment range 10^{10}–10^{15} Nm. *Kanamori and Rivera* [2004], using a wider moment range data set ($10^{10} \leq M_o \leq 10^{19}$ Nm) conclude that static stress drop and rupture velocity can scale differently for small and large earthquakes, and in particular stress drop could not necessarily to be scale independent, although this scale independence is often implied. On the other side, since the active slipping surface on a fault at a given time is controlled by slip duration or rise-time (τ) parameter, the hypothesis that fracture area Σ scales with earthquake magnitude would imply a dependence of rise-time with magnitude. Very recently *Olson and Allen* [2005] advanced the hypothesis that the predominant period parameter τ_p is correlated to the slip duration in the early stages of the rupture. The observed correlation of τ_p with magnitude, would therefore be an evidence that earthquake size scales with rise-time ($\tau \propto L/v_r$) in the initial stage of ruptures, also linked through L to the energy flow G defined above.

References

Aki, K., and P. Richards (1980), *Quantitative Seismology*, W. H. Freeman, New York.

Allen, R. M., and H. Kanamori (2003), The potential for earthquake early warning in southern California, *Science*, *300*, 786–789.

Ambraseys, N., P. Smit, J. Douglas, B. Margaris, R. Sigbjornsson, S. Olafsson, P. Suhadolc, and G. Costa (2004), Internet site for European strong-motion data, *Boll. Geofis. Teor. Appl.*, *45*, 113–129.

Beeler, N. M., T. F. Wong, and S. H. Hickman (2003), On the expected relationships among apparent stress, static stress drop, effective shear fracture energy, and efficiency, *Bull. Seismol. Soc. Am.*, *93*(3), 1381–1389.

Broberg, K. B. (1999), *Cracks and Fractures*, Elsevier, New York.

Brune, J. N. (1970), Tectonic stress and the spectra of seismic shear waves from earthquakes, *J. Geophys. Res.*, *75*, 4997–5009.

De Natale, G., R. Madariaga, R. Scarpa, and A. Zollo (1987), Source parameter analysis from strong motion records of the Friuli, Italy, earthquake sequence (1976–1977), *Bull. Seismol. Soc. Am.*, *77*(4), 1127–1146.

Gubbins, D. (2004), *Time Series Analysis and Inverse Theory for Geophysicists*, Cambridge Univ. Press, New York.

Horiuchi, S., H. Negishi, K. Abe, A. Kamimura, and Y. Fujinawa (2005), An automatic processing system for broadcasting earthquake alarms, *Bull. Seismol. Soc. Am.*, *95*(2), 708–718.

Kanamori, H. (2006), Real-time seismology and earthquake damage mitigation, *Annu. Rev. Earth Planet. Sci.*, *33*, 195–214.

Kanamori, H., and L. Rivera (2004), Static and dynamic scaling relations for earthquakes and their implications for rupture speed and stress drop, *Bull. Seismol. Soc. Am.*, *94*, 314–319.

Kostrov, B. V. (1964), Selfsimilar problems of propagation of shear cracks, *Appl. Math. Mech.*, *28*(5), 1077–1087.

Nielsen, S. (2006), Can earthquake size be controlled by the initial seconds of rupture?, in *Seismic Early Warning*, edited by P. Gasparini, G. Manfredi, and J. Zschau, Springer, New York, in press.

Olson, E. L., and R. Allen (2005), The deterministic nature of earthquake rupture, *Nature*, *438*, 212–215.

Rydelek, P., and S. Horiuchi (2006), Is earthquake rupture deterministic?, *Nature*, *442*, E5–E6.

Scholz, C. H. (1990), *The Mechanics of Earthquakes and Faulting*, pp. 193–194, Cambridge Univ. Press, New York.

Weber, E., et al. (2006), Development and testing of an advanced monitoring infrastructure (isnet) for seismic early-warning applications in the Campania region of southern Italy, in *Seismic Early Warning*, edited by P. Gasparini, G. Manfredi, and J. Zschau, Springer, New York, in press.

Wu, Y. M., and L. Zhao (2006), Magnitude estimation using the first three seconds p-wave amplitude in earthquake early warning, *Geophys. Res. Lett.*, *33*, L16312, doi:10.1029/2006GL026871.

Zeng, Y., K. Aki, and T. Teng (1993), Mapping of the high-frequency source radiation for the Loma Prieta earthquake, California, *J. Geophys. Res.*, *98*, 11,981–11,993.

———————————

M. Lancieri and A. Zollo, Dipartimento di Scienze Fisiche, Università di Napoli Federico II, Naples I-80125, Italy. (aldo.zollo@na.infn.it)

S. Nielsen, Istituto Nazionale di Geofisica e Vulcanologia, Rome, Italy.